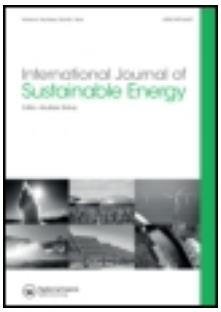

International Journal of Sustainable Energy

Publication details, including instructions for authors and subscription information:
http://www.tandfonline.com/loi/gsol20

Novel integrations of molten salt cavity tubular solar central receiver with existing gas-fuelled conventional steam power plants

Mahmood S. Jamel[ab], A. Abd Rahman[b] & A.H. Shamsuddin[b]

[a] Mechanical Engineering Department, College of Engineering-Basra University, Basra, Iraq

[b] Centre for Renewable Energy, Universiti Tenaga Nasional, Kajang 43000, Selangor, Malaysia

Published online: 15 Nov 2013.

To cite this article: Mahmood S. Jamel, A. Abd Rahman & A.H. Shamsuddin , International Journal of Sustainable Energy (2013): Novel integrations of molten salt cavity tubular solar central receiver with existing gas-fuelled conventional steam power plants, International Journal of Sustainable Energy, DOI: 10.1080/14786451.2013.858159

To link to this article: http://dx.doi.org/10.1080/14786451.2013.858159

International Journal of Sustainable Energy, 2013
http://dx.doi.org/10.1080/14786451.2013.858159

Taylor & Francis
Taylor & Francis Group

Novel integrations of molten salt cavity tubular solar central receiver with existing gas-fuelled conventional steam power plants

Mahmood S. Jamel[a,b*], A. Abd Rahman[b] and A.H. Shamsuddin[b]

[a]*Mechanical Engineering Department, College of Engineering-Basra University, Basra, Iraq;* [b]*Centre for Renewable Energy, Universiti Tenaga Nasional, Kajang 43000, Selangor, Malaysia*

(*Received 21 August 2013; final version received 14 October 2013*)

This paper introduces a new method to integrate the existing equipment of the AL-Hartha steam plant located in Basra, Iraq, using a molten salt cavity tubular solar central receiver (SCR). Cycle Tempo is used to simulate the existing natural gas-fuelled conventional steam power cycle with consideration of the heat and pressure losses. The heliostat field and the central receiver subsystems are coded using MATLAB. The model couples the heat balance with the temperature computation of the receiver walls for calculation and analysis of the thermal losses. The proposed modified codes are capable of calculating heat losses, evaluating the integrated power plant and satisfying a wide range of SCRs. The results are verified against plant data and previous works in the literature and good agreement is obtained. The results show the potential of using a molten salt cavity tubular for low-range temperature to integrate the economizer (EN) and air preheater, as well as the optimum scheme for the integration of the existing plant with an SCR. It is observed that the best improvement for the existing AL-Hartha steam plant and the integrated molten salt cavity tubular SCR can be achieved by integrating EN, and there is about 9.1% saving in gas fuel consumption.

Keywords: hybrid power plants; solar electric-generating system; solar-aided power generation; feedwater preheating; economizer

1. Introduction

With the pressure of global warming and the increase in oil prices, the application of solar energy is getting more and more attention. It is a free and non-depleting energy source with no carbon emissions. Many negative factors such as its relatively low intensity, the change of weather and seasons, etc., make the application of the solar energy inefficient, unsteady, costly, limiting its further applications. An attractive option using the solar thermal to integrate existing steam plants became a reality in the last decades and should be taken as a road map for clean energy in the near future. The early work to use solar thermal with the existing steam plant started in 1975 with Zoschak and Wu (1975) by studying seven methods of absorbing solar energy as the direct thermal input to an 800 MW fossil-fuelled central station steam power plant. Their results showed the combined evaporation and superheating to be the preferred method for hybridisation. Odeh (2003) analysed utilising the solar energy in boiling process arrangement, preheating process

*Corresponding author. Email: mahmood_shaker2005@yahoo.co.uk

arrangement, preheating and boiling process arrangement, he observed that the boiling process arrangement is the most conducive to reduce fossil fuel. Many studies have focused on using solar-aided power generation to replace part of the extraction steam (Pai 1991; Ying and Hu 1999; Gupta and Kaushik 2010; Hu et al. 2010; Suresh, Reddy, and Kolar 2010; Popov 2011; Yang et al. 2011; Jamel, Abd Rahman, and Shamsuddin 2013) and a little on the boiling process in the boiler.

Jun (2011) analysed two types of integration arrangements on the basis of direct steam generation: the arrangement before economizer (EN) and the arrangement after EN. His results indicated that with the same direct solar radiation and solar collector area, the coal and spray water consumption is reduced due to the solar energy which replaces part of the coal supply to the boiler system under the condition of maintaining a constant rated evaporation capacity, and the arrangement before EN has more coal reductions and less spray water reductions than the arrangement after EN, and the arrangement after EN has better system stability in steam production than the arrangement before EN. Little research has been done to examine the boiling process arrangement and air preheating for utilising solar energy in gas-fuelled power plants. This paper tried to do such an analysis using molten salt cavity tubular solar central receiver (SCR) as the solar thermal system .

2. Computational methodology

2.1. *Modelling of the existing steam cycle*

The selected case study is the AL-Hartha steam power plant located in Basra, Iraq. The superheated steam enters the two-stage single reheat steam turbine at 541°C/125 bar and 541°C/36.77 bar, for the high- and intermediate-pressure stages, respectively. Steam enters the low-pressure stage with a pressure of 6.934 bar and the condenser pressure is 80 kPa. The simulation process is done using Cycle Tempo as shown in Figure 1.

2.2. *Modelling of the heliostat field subsystem*

A simple model is implemented to determine the solar position described in Chong and Tan (2011). The overall field efficiency η_{field} is expressed by the following equation:

$$\eta_{\text{field}} = \eta_{\cos}\eta_{\text{atten}}\eta_{\text{Blok \& shadow}}\eta_{\text{reft}}\eta_{\text{spill}}. \tag{1}$$

The cosine efficiency of a heliostat is equal to the cosine of incidence angle θ relative to the heliostat centre and is given by $\eta_{\cos} = \cos\theta$. The atmospheric attenuation efficiency can be calculated simply as a function of the distance between the heliostat and the receiver in metres (Schmitz et al. 2006):

$$\eta_{\text{atten}} = 0.99321 - 0.001176S + 1.97 \times 10^{-8}S^2, \; S \leq 1000\,\text{m}, \tag{2}$$

$$\eta_{\text{atten}} = \text{e}^{-0.0001106S}, \; S \leq 1000\,\text{m}, \tag{3}$$

where S is the distance between the heliostat and the receiver. The actual mirror reflectivity is taken as $\eta_{\text{reft}} = 0.836$. The consideration of the heliostats never overlapping is considered here; thus, the shading and blocking losses are equal zero or $\eta_{\text{Blok \& shadow}} = 1$. In addition, because the scope of the present study considers only the total area generated, there is no need to describe the field layout and, therefore, there is no need to include such minor losses; thus, $\eta_{\text{spill}} = 1$.

The incident solar radiation Q_{solar} is proportional to the total area of the heliostat field and can be expressed as the product of the direct normal irradiance for the surface hit by the sunlight:

$$Q_{\text{solar}} = A_{\text{field}}\text{DNI}. \tag{4}$$

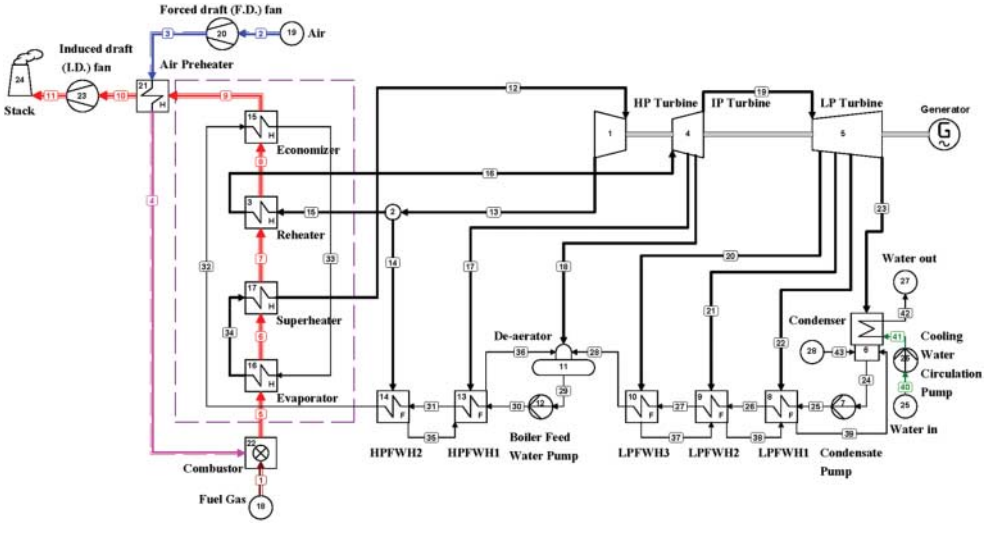

Figure 1. Schematic diagram for existing 200 MW unit at AL-Hartha Steam power plant.

The incident power into the receiver aperture from the heliostat field (power to the receiver) Q_{rec}, is calculated by (Yao et al. 2009):

$$Q_{\text{rec}} = A_{\text{field}}\text{DNI}\eta_{\text{field}}\Gamma. \tag{5}$$

The exergy E_{solar} associated with the solar irradiation on the heliostat mirror surface Q_{solar} can be expressed as

$$E_{\text{solar}} = Q_{\text{solar}}(1 - T_{\text{a}}/T_{\text{s}}), \tag{6}$$

where T_{S} is the apparent sun temperature as an exergy source and has been taken to be 4500 K (Xu et al. 2011). Similarly, the exergy delivered to the receiver is written as

$$E_{\text{rec}} = Q_{\text{rec}}(1 - T_{\text{a}}/T_{\text{s}}). \tag{7}$$

Energy losses for the heliostat field are

$$Q_{\text{loss.H}} = Q_{\text{solar}} - Q_{\text{rec}}. \tag{8}$$

The exergy losses for the heliostat field IR_{H} are

$$\text{IR}_{\text{H}} = E_{\text{solar}} - E_{\text{rec}}. \tag{9}$$

The energy efficiency and exergy efficiency of the heliostat field subsystem are given by

$$\eta_{\text{I.H}} = \frac{Q_{\text{rec}}}{Q_{\text{solar}}}, \tag{10}$$

$$\eta_{\text{II.H}} = \frac{E_{\text{rec}}}{E_{\text{solar}}}. \tag{11}$$

2.3. *Modelling of the central receiver subsystem*

The purpose of the current study is the integration of SCR to an existing steam plant. With such technologies and as the limitations of the design and working conditions for these existing plants becoming older, there is no need to use advanced technology and higher temperatures provided by volumetric receivers. In addition, the latter are an underdeveloped technology and the superheated steam receiver has poor steam heat-transfer capabilities (Kribus, Ries, and Spirkl 1996; Buck et al. 2006). Among the available types of SCRs, a cavity tubular receiver with molten salt as the working fluid was selected as offering the potential to be one of the most cost effective and safe receivers. This type of receiver is divided into two parts: stainless steel tubes and flowing molten salt in tubes. The analysis here is based on the cavity receiver. In operation, the receiver absorbs the insolation $Q_{\text{rec}}$and transports part of the energy to the molten salt flowing through it. The remainder of the energy is lost to the environment by convective, emissive, reflective and conductive heat losses and is expressed by the receiver total heat loss $Q_{\text{rec.totloss}}$. The energy balance and exergy balance for the central receiver are

$$Q_{\text{rec}} = Q_{\text{rec.abs}} + Q_{\text{rec.totloss}}, \tag{12}$$

$$E_{\text{rec}} = E_{\text{rec.abs}} + E_{\text{rec.totloss}} + IR_{\text{rec}}, \tag{13}$$

where $Q_{\text{rec.abs}}$ is the receiver absorbed heat, this parameter is taken as the design point for receiver and calculated by

$$Q_{\text{rec.abs}} = \dot{m}\Delta h = \dot{m}\, Cp_{\text{ms}}(T_{\text{ms.out}} - T_{\text{ms.in}}) \tag{14}$$

It is important to mention here that the molten salt temperatures are compatible with temperature difference for the integrated part. The exergy loss associated with the heat loss is expressed as

$$E_{\text{rec.totloss}} = Q_{\text{rec.totloss}}(1 - T_{\text{a}}/T_{\text{rec.sur}}), \tag{15}$$

while the useful exergy absorbed by flowing heat-transfer fluid are expressed by

$$E_{\text{rec.abs}} = \dot{m}_{\text{ms}}\, Cp_{\text{ms}}(T_{\text{ms.out}} - T_{\text{ms.in}}) - T_{\text{a}}\,\text{In}(T_{\text{ms.out}}/T_{\text{ms.in}}) \tag{16}$$

then, the energy efficiency and exergy efficiency of the central receiver subsystem can be defined as

$$\eta_{\text{I.rec}} = \frac{Q_{\text{rec.abs}}}{Q_{\text{rec}}}, \tag{17}$$

$$\eta_{\text{II.rec}} = \frac{E_{\text{rec.abs}}}{E_{\text{rec}}}. \tag{18}$$

A modified thermal model for the molten salt cavity receiver is used here to calculate total heat losses, the detail model and parameters can be reviewed in Li et al. (2010):

$$Q_{\text{rec.totloss}} = Q_{\text{rec.conv}} + Q_{\text{rec.em}} + Q_{\text{rec.ref}} + Q_{\text{rec.con}}. \tag{19}$$

3. Results and discussion

3.1. *Results validation*

The evaluation criteria for suggested plant modification in the present analysis are based on the energy balance and exergy balance of each subsystem. The steam cycle validated through

simulating other operating units that are exactly similar to the damaged units using Cycle Tempo for full load operation is shown in Figure 1. This simulated cycle is verified with practical data collected from the actual plant and good results are obtained.

The analysis for the central receiver is based on a thermal model, which is modified from a validated model developed by Li et al. (2010) and Xu et al. (2011). To validate the modification, the present model was used to calculate the thermal performance of the Sandia National Laboratories' molten salt electric experiment based on the parameters provided in Li et al. (2010). The calculated energy efficiency of the receiver is 86.66%, which gives acceptable agreement with Li et al. (2010) and Xu et al. (2011). While for the heliostat field subsystem, the calculated efficiencies agree with the results of Yao et al. (2009); therefore, the paper's results are reasonable and useful for guiding the design and integration of SCR. Overall, the computational work has been split into three schemes:

Scheme A: Base case calculations in the design mode for existing gas-fuel-fired power plant.

Scheme B: Design calculations of Scheme A plant with EN replaced by solar field. This case assumes solar feedwater preheating from about 242–297°C.

Scheme C: Design calculations of Scheme A plant with air preheater (AH) replaced by solar field. This case assumes air preheating from about 27.75–300°C.

The temperatures range assumptions for Schemes B and C refer to the plant design temperatures at full load and standard conditions (25°C and 1.013 bar), and as the current study proposed zero modification for the existing plant, therefore the temperature ranges of hot flue gases through EN and AH required for solar field design were kept the same as designed to avoid any possible modification in boiler ducting and materials. Scheme B discussed the impact of EN integration with molten salt cavity tubular SCR with feed water temperature range from 242°C to 297°C on the existing EN of gas-fuelled fired power plant. The feed water from heaters is received by the boiler, going through the EN first. The integration scheme proposed adds the water to the additional heat exchanger added in parallel with the fired EN in order to receive the heat from molten salt instead of the flue gas, and then the hot water moves to the next part of the boiler that is the evaporator as shown in Figure 2. Such an integration allows for hybrid or stand-alone operation, but there is need to add some heat exchangers and a modified piping system. While Scheme C proposed integration of SCR to AH. In this arrangement, a new heat exchanger is put in parallel with the AH section of the steam generator as shown in Figure 3. The air required for combustion is preheated from ambient air temperature up to 300°C, the plant design temperature during the period of solar input to avoid any possible modification like changing ducting materials for the existing plant when using higher preheating temperatures. With the conventional AH not in service, the energy in the high-temperature flue gas discharged directly to the stack is not recovered and the efficiency of the steam generator is reduced. Such suggested operation modes have not affected the other components in the power plant, achieving the first target of simple modification and low level of complexity.

The specified temperature ranges for both schemes are used as a design temperatures for central receiver. The SCR model compatible with Cycle Tempo was run in thermodynamic and engineering design modes to evaluate performance, calculate solar field capacity and basic configuration for each schemes. The selected operation mode for such an integration is the fuel conservation mode in which the gross power output is constant. The effect of such an integration on the plant energy and exergy bases in fuel conservation mode was discussed and evaluated.

3.2. *Comparison between integration schemes*

The aim of the current study is to determine the best possible integration scheme and the impact of such an integration on both existing steam cycle and SCR systems. The stream data of Schemes A and B (corresponding to Figures 1 and 2) are presented in Table 1. The stream data of Schemes

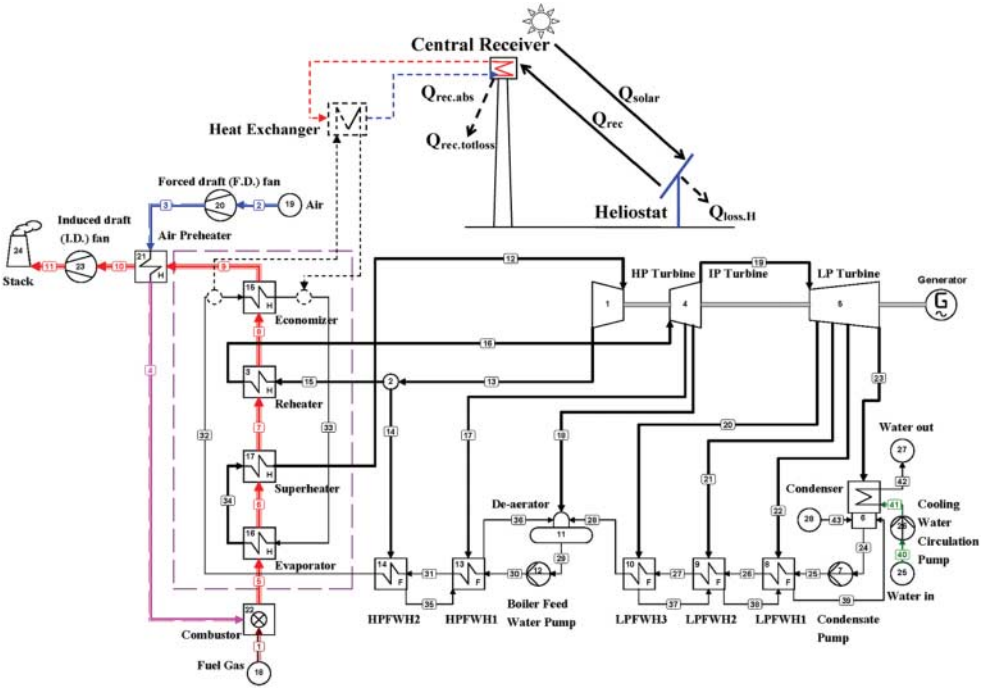

Figure 2. Schematic representation of proposed integration of EN with molten salt cavity tubular SCR.

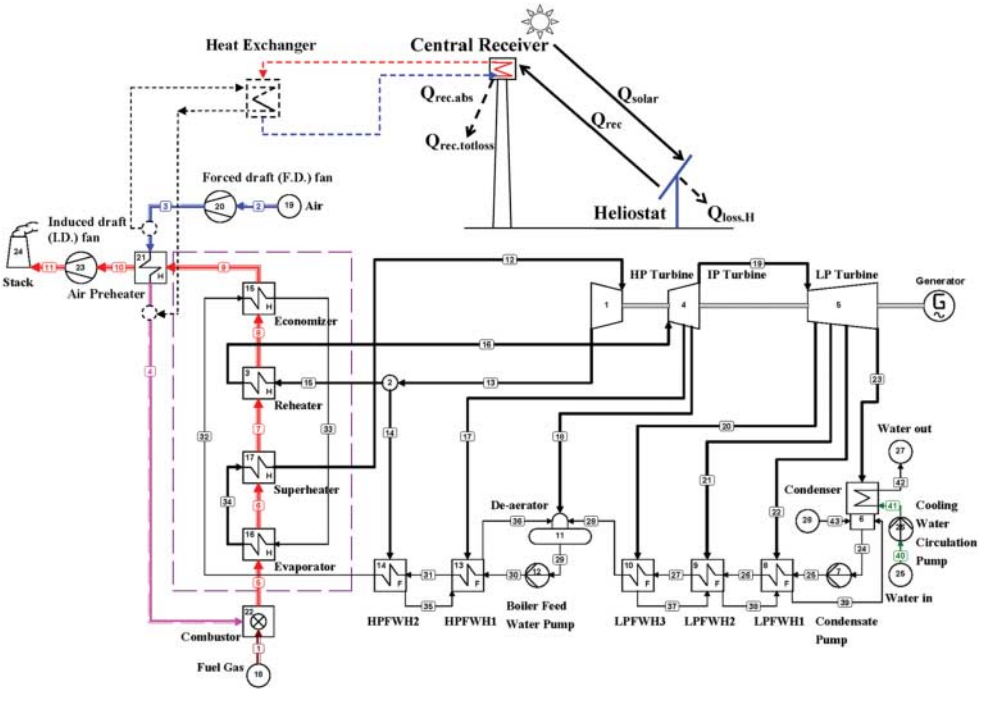

Figure 3. Schematic representation of proposed integration of AH with molten salt cavity tubular SCR.

Table 1. Stream data for existing and integrated gas-fuelled fired power plant for Scheme A and B.

Outlet pipe as Figure 2	Mass flow (kg/s)	Pressure (bar)	Temperature (°C)	Total energy flow (MW_{th})	Total exergy flow (MW_{th})
Natural gas					
1	10.9(9.9)	1.031	25	556.2(551.9)	523.4(519.3)
Air/flue gases					
2	236.2(234.4)	1.013	25	3.9(3.8)	0.2(0.2)
3	236.2(234.4)	1.036	27.7	4.5(4.5)	0.6(0.6)
4	236.2(234.4)	1.031	300	70.5(70.0)	20.2(20.0)
5	247.2(244.3)	1.031	1811.8	622.7(622.2)	407.7(404.5)
6	247.2(244.3)	1.011	1115.3(1057.9)	407.5(405.5)	225.1(213.9)
7	247.2(244.3)	1.001	705.8(686.9)	286.6(274.4)	132.6(116.8)
8	247.2(244.3)	1.000	512.8(512.8)	226.6(215.9)	90.5(78.1)
9 (NA)	247.2(244.3)	0.980	350	148.4	43.1
10	247.2(244.3)	0.971	112.6(284.9)	82.4(143.1)	16.5(37.5)
11	247.2(244.3)	1.060	124.1(299.1)	85.5(147.5)	19.1(41.4)
Water/steam					
12	173.7	124.8	538.3	581.4	259.0
13	173.7	38.7	379.5	532.9	204.5
14	17.9	36.8	377.8	54.9	20.9
15	155.8	36.8	377.8	478.0	182.4
16	155.8	34.9	540.2	536.5	215.9
17	7.1	14.7	420.2	22.6	7.9
18	6.2	6.7	318.5	18.7	5.6
19	142.5	6.9	315.6	426.4	129.6
20	6.3	3.2	235.4	18.0	4.6
21	7.0	1.4	156.1	18.8	3.9
22	8.6	0.48	80.2	21.8	3.3
23	120.4	0.090	43.8	280.7	17.2
24	142.5	0.080	41.5	11.7	0.3
25	142.5	6.8	43.8	11.8	0.4
26	142.5	6.8	77.2	31.7	2.6
27	142.5	6.7	107.0	49.6	5.9
28	142.5	6.7	133.0	65.3	9.8
29	173.7	6.7	163.6	102.6	18.6
30	173.7	154	166.0	105.9	21.6
31	173.7	146.8	194.4	127.3	28.9
32	173.7	146.7	242.4	165.0	43.8
33	173.7	145.1	296.9	212.2	65.2
34	173.7	131.4	340.4	450.1	185.5
35	17.9	14.71	197.3	17.2	4.3
36	24.9	6.766	163.5	18.4	3.8
37	6.3	1.436	110.0	2.3	0.3
38	13.3	0.478	80.2	3.2	0.2
39	22.0	0.090	43.8	5.1	0.2
40	8201.6	1.013	25	34.3	0
41	8201.6	1.27	25	34.5	0.2
42	8201.6	1.07	33	30.7	4.6

A and C (corresponding to Figures 1 and 3) are presented in Table 2. In these tables, air and flue gas temperatures (outlet pipe points from 1 to 11) in the boiler change according to the amount of heat capacity and temperature range of replaced parts by SCR. As a result, the flue gas stack temperature for both the proposed schemes was higher than the same temperatures of the basic Scheme A. This assumption was carried out for both Schemes B and C.

The heat from the SCR has an effect on the performance of the boiler. The gas fuel firing rate is reduced to account for the reduced heat absorption of EN and AH sections as shown in Figure 4. The calculations for Scheme B are based on the constant rated evaporation capacity. According to the calculation results, the gas fuel consumption has been reduced with a percentage of 9.1% for Scheme B.

Table 2. Stream data for existing and integrated gas-fuelled fired power plant for Scheme A and C.

Outlet pipe as Figure 3	Mass flow (kg/s)	Pressure (bar)	Temperature (°C)	Total energy flow (MW_{th})	Total exergy flow (MW_{th})
Natural gas					
1	10.9 (9.5)	1.031	25	556.2(550.1)	523.4(517.3)
Air/flue gases					
2	236.2 (234.4)	1.013	25	3.9(3.8)	0.2(0.2)
3	236.2 (234.4)	1.036	27.7	4.5(4.5)	0.6(0.6)
4(NA)	236.2 (234.4)	1.031	300	70.5	20.2
5	247.2 (243.9)	1.031	1811.8(1630	622.7(610.5)	407.7(402.5)
6	247.2 (243.9)	1.011	1115.3(1019.2)	407.5(404.0)	225.1(208.8)
7	247.2 (243.9)	1.001	705.8(660.1)	286.6(272.8)	132.6(112.72)
8	247.2 (243.9)	1.000	512.8(491.5)	226.6(214.4)	90.5(74.5)
9	247.2 (243.9)	0.980	350	148.4(146.2)	43.1(41.9)
10(NA)	247.2 (243.9)	0.971	112.6	82.4	16.5
11	247.2 (243.9)	1.060	124.1(363	85.5(171.7)	19.1(51.4)

Note: Values in parentheses refer to integrated plant with SCR-Scheme C; NA, not applicable. Water/Steam cycle remain fixed as in Table 1.

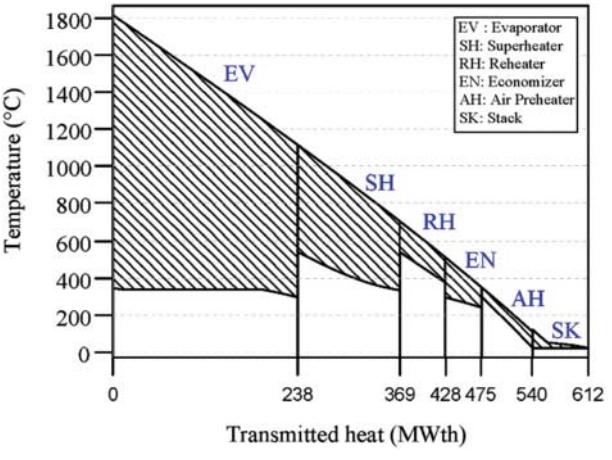

Figure 4. The amount of heat transmitted for each part of boiler.

While for Scheme C, the calculations are based on constant air flow rate passed AH with keeping forced draft fan as existing for better heat transfer and to avoid any possible modification to existing equipment. Again, there is fuel saving of about 13% for Scheme C. The reduction of fuel consumption for both schemes is gained due to the integration of the solar energy into the boiler system, achieving the second targets of energy saving. It is clear here that the fuel consumption for Scheme C is larger than Scheme B, this is due to the temperature ranges and amount of heat transmitted for each section as shown in Figure 4. This does not mean that Scheme C is better than Scheme B. The area of heliostats for Scheme C is about 126,365 m^2, while for Scheme B it is lower. AH is the last heat exchanging section in the boiler and when integrated with solar field there is no chance for heat absorption from high-temperature flue gases that exit the boiler. This leads to high exhausted temperature reaching up to 363.3°C for selected conditions. Due to this effect, there is very sharp reduction in energy and exergy efficiencies for the existing plant when integrated with Scheme C in spite of the highest value of fuel reduction.

For the integrated SCR, there are some attractive results. The main result is the ability of the integration of SCR for a low range of working temperatures. Here, for evaluation purposes, SCR

Table 3. Effect of performance factors on the existing plant.

Subsystem	Performance parameter	Schemes A	Scheme B	Scheme C
Existing gas fuel steam cycle	Net absorbed energy (MW_{th})	500.5	555.7	577.3
	Net unit capacity (MW)	187.1	184.9	184.9
	Net energy efficiency (%)	37.4	33.4	32.0
	Net exergy efficiency (%)	36.1	30.9	30.9
The heliostat field subsystem	The incident solar radiation(MW_{th})	0	77.6	107.4
	The exergy associated with the solar irradiation (MW_{th})	0	72.5	100.4
	Heliostat field heat losses; (MW_{th})	0	28.1	38.8
	Exergy losses for the heliostat field (MW_{th})	0	26.2	36.2
	The energy efficiency of the heliostat field (%)	0	63.8	63.8
	The exergy efficiency of the heliostat field (%)	0	63.8	63.8
	The area of heliostat field (m^2)	0	91325	126365
The receiver subsystem	The incident power into receiver aperture from the heliostat field (MW_{th})	0	49.6	68.6
	The Receiver total heat loss (MW_{th})	0	2.3	3.1
	The exergy delivered to the receiver (kW_{th})	0	46.3	64.1
	The exergy loss associated with the heat loss(MW_{th})	0	1.4	1.9
	The exergy losses for the central receiver (MW_{th})	0	27	43.1
	The energy efficiency of the receiver (%)	0	95.3	95.4
	The exergy efficiency of the receiver (%)	0	63.5	73.9
The integrated Cycle	Natural gas consumption (kg/s)	10.9	9.9	9.5
	Natural gas conservation (%)	0	9.1	13

Table 4. Properties of the base case solar tower power plant.

Subsystem	Properties	Values unit
Heliostat field	Beam radiation (Direct normal irradiance)	850 W/m^2
	The latitude	30.677°
	The longitude	47.816°
	Day number	196
	The distance between the heliostat and the receiver	1000 m
	The radial distance between heliostat and	55 m
	The height of the heliostat	7 m
	The target height	95 m
	The facing angle	63°
	Local time	14 h
Central receiver	Aperture area	16.96 m^2
	Inlet temperature of molten salt	290°C
	Outlet temperature of molten salt	560°C
	View factor	0.8
	Tube diameter	0.019 m
	Tube thickness	0.00165 m
	Emissivity	0.8
	Aperture height	6 m
	Reflectivity	0.04
	Conductivity of tube material	19.7 W/mK
	Conductivity of insulation	40 W/mK
	Insulation layer thickness	0.07
	Wind velocity	5.0 m/s

is divided into two subsystems: the heliostat field and the central receiver. The effects of such an integration, as well as the change of performance parameters, are shown in Table 3. For the heliostat field, the field energy and exergy efficiencies are constant at 63.8% for all cases. This is

because it is related to the selected site, date, time and other technical inputs, shown in Table 4, which are held constant for all the selected schemes. The heliostat field heat losses for Scheme C are more than in Scheme B. This is because the heliostat area is greater in Scheme C. The greater heat-transfer area leads to greater heat losses and exergy losses. However, for the central receiver, there is a very slight improvement in the high values of receiver energy and exergy efficiencies; the energy efficiency increases from 95.3% for Scheme B to 95.4% for Scheme C, whereas the exergy efficiency of the receiver increases from 63.5% for Scheme B to 73.9% for Scheme C. To analyse this, it is important initially to fix the operational mode of the receiver. The selected mode is fixed for molten salt output temperatures for all selected schemes, which offers safer operation compared with the other modes (Li et al. 2010). The receiver absorbed heat $Q_{\text{rec.abs}}$ is taken here as a design point for the receiver, as mentioned $Q_{\text{rec.abs}}$ is higher for Scheme C compared with Scheme B, and receiver efficiency increases with increasing $Q_{\text{rec.abs}}$. Therefore, it is logical to see some improvements in receiver energy efficiency for Scheme C. In general, Scheme B has a potential to become the best possible integration scheme over Scheme C due to the technical benefits and the need for simple modification for the existing plant although Scheme C has the best performance impact.

4. Conclusions

Two new schemes for the integration of the AL-Hartha steam plant with a molten salt cavity tubular SCR are proposed in this paper. These schemes are evaluated through a modified model for both the existing power plant and the integrated SCR in order to determine the best solution offering the highest performance. The use of a molten salt cavity tubular SCR for low-range temperature feedwater preheating at EN and AH was verified. As well as the best scheme for integration with the existing plant, the SCR that offers the highest performance was also investigated. It is shown that maximum improvement for the existing AL-Hartha steam plant and the integrated molten salt cavity tubular SCR was obtained. The obtained results clearly indicate Scheme C as the worst scenario for the proposed solar repowering for selected options in spite of their best performance and Scheme B has a potential to be the best possible integration scheme.

Acknowledgements

The authors would like to thank the Energy Technology Section, Delft University of Technology, The Netherlands for licensing a copy of Cycle Tempo and Mr Mark Roest for providing technical support. Also, thanks go to the staff of AL-Hartha steam plant for their efforts in providing plant technical data.

Abbreviation

DNI	direct normal irradiance

Nomenclature

F_r	view factor
A	area (m^2)
Cp	specific heat at constant pressure (W/m^2 K)
d	diameter (m)
h	heat-transfer coefficient (W/m^2 K)
k	conductivity (W/m K)
m	mass flow rate (kg/s)
Q	heat (kW)
S	distance from the heliostat and the receiver (m)
T	temperature (°C)

Greek symbols

ε	emissivity
Γ	the fraction of the field in track
η	efficiency
σ	Stefan–Boltzmann constant 5.67×10^{-8} (W/m^2 K^4)

Subscript

a	ambient
avg	average
air	air
con	conductive heat loss
abs	absorbed energy
conv	convective heat loss
in	inner tube or inlet
em	emissive heat loss
fc	forced convection
insu	insulation
isni	inner side of receiver
ms	molten salt
loss	heat loss
out	outer tube or outlet
nc	natural convection
rec	receiver
ref	reflective heat loss
s	solar
sur	surface
totloss	total heat loss
tube	receiver absorber tube
w	wall surface

References

Buck, R., C. Barth, M. Eck, and W.-D. Steinmann. 2006. "Dual-Receiver Concept for Solar Towers." *Solar Energy* 80 (10): 1249–1254. Accessed http://www.sciencedirect.com/science/article/pii/S0038092X05002197

Chong, K. K., and M. H. Tan. 2011. "Range of Motion Study for Two Different Sun-Tracking Methods in the Application of Heliostat Field." *Solar Energy* 85 (9): 1837–1850. Accessed http://www.sciencedirect.com/science/article/pii/S0038092X11001447

Gupta, M. K., and S. C. Kaushik. 2010. "Exergy Analysis and Investigation for Various Feed Water Heaters of Direct Steam Generation Solar–Thermal Power Plant." *Renewable Energy* 35 (6): 1228–1235. Accessed http://www.sciencedirect.com/science/article/pii/S0960148109004029

Hu, E., Y. Yang, A. Nishimura, F. Yilmaz, and A. Kouzani. 2010. "Solar Thermal Aided Power Generation." *Applied Energy* 87 (9): 2881–2885. Accessed http://www.sciencedirect.com/science/article/pii/S0306261909004693

Jamel, M. S., A. Abd Rahman, and A. H. Shamsuddin. 2013. "Advances in the Integration of Solar Thermal Energy with Conventional and Non-Conventional Power Plants." *Renewable and Sustainable Energy Reviews* 20 (0): 71–81. Accessed http://www.sciencedirect.com/science/article/pii/S1364032112005692

Jun, Z. 2011. "Analysis of Solar Aided Steam Production in a Pulverized Coal Boilered." Power and energy engineering conference (APPEEC), 2011 Asia-Pacific, 1–4. Accessed http://ieeexplore.ieee.org/stamp/stamp.jsp?tp=&arnumber=5748488

Kribus, A., H. Ries, and W. Spirkl. 1996. "Inherent limitations of Volumetric Solar Receivers." *Journal of Solar Energy Engineering* 118 (3): 151–155. Accessed http://link.aip.org/link/?SLE/118/151/1; http://dx.doi.org/10.1115/1.2870891

Li, X., W. Kong, Z. Wang, C. Chang, and F. Bai. 2010. "Thermal Model and Thermodynamic Performance of Molten Salt Cavity Receiver." *Renewable Energy* 35 (5): 981–988. Accessed http://www.sciencedirect.com/science/article/pii/S0960148109004935

Odeh, S. D. 2003. "Unified Model of Solar Thermal Electric Generation Systems." *Renewable Energy* 28 (5): 755–767. Accessed http://www.sciencedirect.com/science/article/pii/S0960148102000447

Pai, B. R. 1991. "Augmentation of Thermal Power Stations with Solar Energy." *Sadhana* 16 (1): 59–74. Accessed http://dx.doi.org/10.1007/BF02811380

Popov, D. 2011. "An Option for Solar Thermal Repowering of Fossil Fuel Fired Power Plants." *Solar Energy* 85 (2): 344–349. Accessed http://www.sciencedirect.com/science/article/pii/S0038092X10003579

Schmitz, M., P. Schwarzbözl, R. Buck, and R. Pitz-Paal. 2006. "Assessment of the Potential Improvement Due to Multiple Apertures in Central Receiver Systems with Secondary Concentrators." *Solar Energy* 80 (1): 111–120. Accessed http://www.sciencedirect.com/science/article/pii/S0038092X05000903

Suresh, M. V. J. J., K. S. Reddy, and A. K. Kolar. 2010. "4-e (Energy, Exergy, Environment, and Economic) Analysis of Solar Thermal Aided Coal-Fired Power Plants." *Energy for Sustainable Development* 14 (4): 267–279. Accessed http://www.sciencedirect.com/science/article/pii/S0973082610000517

Xu, C., Z. Wang, X. Li, and F. Sun. 2011. "Energy and Exergy Analysis of Solar Power Tower Plants." *Applied Thermal Engineering* 31 (17–18): 3904–3913. Accessed http://www.sciencedirect.com/science/article/pii/S135943111100398X

Yang, Y., Q. Yan, R. Zhai, A. Kouzani, and E. Hu. 2011. "An Efficient Way to Use Medium-or-Low Temperature Solar Heat for Power Generation – Integration Into Conventional Power Plant." *Applied Thermal Engineering* 31 (2–3): 157–162. Accessed http://www.sciencedirect.com/science/article/pii/S1359431110003637

Yao, Z., Z. Wang, Z. Lu, and X. Wei. 2009. "Modeling and Simulation of the Pioneer 1 MW Solar Thermal Central Receiver System in China." *Renewable Energy* 34 (11): 2437–2446. Accessed http://www.sciencedirect.com/science/article/pii/S0960148109000937

Ying, Y., and E. J. Hu. 1999. "Thermodynamic Advantages of Using Solar Energy in the Regenerative Rankine Power Plant." *Applied Thermal Engineering* 19 (11): 1173–1180. Accessed http://www.sciencedirect.com/science/article/pii/S1359431198001148

Zoschak, R. J., and S. F. Wu. 1975. "Studies of the Direct Input of Solar Energy to a Fossil-Fuelled Central Station Steam Power Plant." *Solar Energy* 17 (5): 297–305. Accessed http://www.sciencedirect.com/science/article/pii/0038092X7590047X